Chinese Chemical Letters 33 (2022) 943–947

Contents lists available at ScienceDirect

Chinese Chemical Letters

journal homepage: www.elsevier.com/locate/cclet

Sea-urchin-like ReS_2 nanosheets with charge edge-collection effect as a novel cocatalyst for high-efficiency photocatalytic H_2 evolution

Bo Lin[a,1], Bowen Ma[a,1], Jiangang Chen[a], Yao Zhou[b,*], Jiadong Zhou[c], Xiaoqing Yan[d], Chao Xue[e], Xiao Luo[a], Qing Liu[a], Jinyong Wang[a], Renji Bian[a], Guidong Yang[d,*], Fucai Liu[a,*]

[a] School of Optoelectronic Science and Engineering, University of Electronic Science and Technology of China, Chengdu 611731, China
[b] School of Physical and Mathematical Sciences, Nanyang Technological University, Singapore 637371, Singapore
[c] Key Lab of Advanced Optoelectronic Quantum Architecture and Measurement (Ministry of Education), Beijing Key Lab of Nanophotonics & Ultrafine Optoelectronic Systems, and School of Physics, Beijing Institute of Technology, Beijing 100081, China
[d] XJTU-Oxford International Joint Laboratory for Catalysis, School of Chemical Engineering and Technology, Xi'an Jiaotong University, Xi'an 710049, China
[e] State Centre for International Cooperation on Designer Low-carbon and Environmental Materials (CDLCEM), School of Materials Science and Engineering, Zhengzhou University, Zhengzhou 450001, China

ARTICLE INFO

Article history:
Received 23 April 2021
Revised 2 June 2021
Accepted 6 July 2021
Available online 14 July 2021

Keywords:
Sea-urchin-like ReS_2 nanosheets
Charge edge-collection effect
2D planar edges/tips
Charge transfer
Photocatalytic H_2 evolution

ABSTRACT

The recombination of charge carriers arriving from the random charge movement in semiconductor photocatalysts greatly limits the practical application of solar-driven H_2 evolution. The design of photocatalytic systems with spatially oriented charge-transfer is a promising route to achieve high charge-separation efficiency for photocatalysts. Herein, novel sea-urchin-like ReS_2 nanosheet/TiO_2 nanoparticle heterojunctions (SURTHs) are constructed. The unique sea-urchin-like structure endows the ReS_2 cocatalyst with an unusual charge edge-collection effect, which leads to a significant acceleration of charge separation and transfer, as evidenced by the well-designed selective photodeposition of Pt quantum dots in SURTHs. The markedly improved charge transfer capacity contributes to a high photocatalytic H_2 evolution rate of 3.71 mmol h^{-1} g^{-1} for SURTHs (an apparent quantum efficiency (AQE) of 16.09%), up to 231.9 times by contrast with that of P25 TiO_2. This work would provide a new platform for designing the high-efficiency cocatalyst/photocatalyst system with excellent charge transfer capacity.

Solar-driven H_2 generation from water is an attractive route to deal with the global energy crisis [1–3], yet the high recombination rate of charge carriers arriving from the random charge movement in semiconductor photocatalysts greatly limits its practical application [4–6]. One effective approach to break this bottleneck is the use of cocatalysts, which can provide massive adsorption and reaction active sites for water molecules, facilitate the separation and migration of charges, thus improving the overall photocatalytic quantum efficiency [7,8]. In terms of the choice of cocatalysts, noble metals represented by Pt, Pd, and Au have been considered to be the highly-active cocatalysts for photocatalytic H_2 generation [9]. However, the high cost and scarcity of noble-metal cocatalysts limit their future applications. Hence, it is necessary to develop the alternative cocatalysts with high activity and low cost. Recently, transition metal dichalcogenides (TMDs) have aroused keen interests owing to their outstanding optical and electronic properties, high aspect ratio, and low cost [10–12]. In the community of TMDs, a new member of ReS_2 has many unique advantages, including large surface area, highly active basal-plane sites, and structural anisotropy, which enable it to be an ideal cocatalyst for photocatalytic H_2 evolution [13,14].

Except for the types of cocatalysts, the morphology and structure of cocatalysts is another important factor to influence the photocatalytic performance for H_2 evolution. The common morphologies of cocatalysts include nanoparticles, nanospheres, flakes, clusters, nanotubes, and quantum dots, *etc.* The loading of cocatalysts with the specific morphologies presented above can improve the charge transfer efficiency and boost the photocatalytic H_2 generation activity for semiconductor photocatalysts [15–20]. Apart from the common structures, inspired by nature, the mimic nature-like nanostructures have been introduced into nanomaterials to achieve high-efficiency charge separation and migration in photocatalytic H_2 evolution, such as fish-scale-like nanostructure, butterfly-wing-like nanostructure, and ginkgo-leaf-like nanostructure [6,21,22]. Among diverse nature-like nanostructures, the sea-

* Corresponding authors.
E-mail addresses: zhouyao@ntu.edu.sg (Y. Zhou), guidongyang@mail.xjtu.edu.cn (G. Yang), fucailiu@uestc.edu.cn (F. Liu).
[1] These authors contributed equally to this work.

https://doi.org/10.1016/j.cclet.2021.07.015
1001-8417/

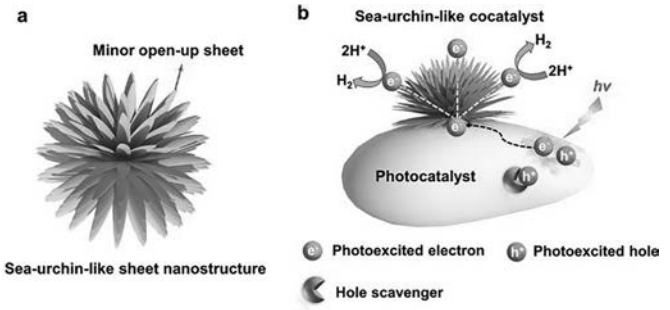

Scheme 1. (a) Schematic of sea-urchin-like sheet nanostructure. (b) Schematic of the sea-urchin-like cocatalyst with the charge edge-collection effect loaded on the photocatalyst for H_2 evolution.

urchin-like sheet nanostructure is an interesting and superexcellent structure for cocatalysts. As shown in Scheme 1a, the numerous minor open-up sheets with sharp edges are similar to the spines of a sea urchin, which can not only provide plenty of adsorption and reaction active sites to speed up the H_2 evolution reaction, but also induce a fast charge transfer and collection at the tips of minor sheets like the lightning rod effect [15]. Therefore, if well developed, the construction of sea-urchin-like structured cocatalysts with the charge edge-collection effect would open a new window for the design of cocatalyst/photocatalyst system with high photocatalytic H_2 evolution performance (Scheme 1b).

Herein, we construct novel sea-urchin-like ReS_2 nanosheet/TiO_2 nanoparticle heterojunctions (shorthand for SURTHs) by a simple one-step hydrothermal method. By contrast with the bulk ReS_2 cocatalyst constituted by massive agglomerated nanoparticles or nanosheets, the sea-urchin-like ReS_2 cocatalyst displays the unusual charge edge-collection effect, thus leading to a significantly accelerated charge transfer and a high photocatalytic H_2 evolution rate of 3.71 mmol h^{-1} g^{-1} (an apparent quantum efficiency (AQE) of 16.09%) for SURTHs, up to 231.9 times in comparison with that of P25 TiO_2.

The overall formation procedure of SURTHs is illustrated in Fig. 1a. Initially, P25 TiO_2 nanoparticles were dispersed into an aqueous solution containing NH_4ReO_4 and TAA, where the ReO_4^-group absorbed on the surface of TiO_2 nanoparticles. After the hydrothermal treatment at 250 °C, the released S^{2-} from TAA reacted with the ReO_4^- group to generate sea-urchin-like ReS_2 nanosheets, which were anchored on the surface of TiO_2 nanoparticles to form SURTHs. The unique structure of SURTHs was investigated by high-angle annular dark-field scanning transmission electron microscopy (HAADF-STEM) and transmission electron microscopy (TEM). As displayed in Figs. 1b–e, 3D open-up interconnecting ReS_2 sheets with sharp edges like a sea urchin (a size of ~70 nm) were uniformly loaded on the surface of P25 TiO_2 nanoparticles to form the binary heterojunction. The high-resolution TEM (HRTEM) is performed to further investigate the interface details of sea-urchin-like ReS_2 nanosheet/TiO_2 nanoparticle heterojunctions. As shown in Fig. 1f, the adjacent lattice-fringe spacings of 0.61 and 0.325 nm belong to the (001) reflection plane of triclinic ReS_2 and the (110) reflection plane of rutile TiO_2, respectively. As shown in Fig. 1g, the adjacent lattice-fringe spacings of 0.61 and 0.352 nm are attributed to the (001) reflection plane of triclinic ReS_2 and the (101) reflection plane of anatase TiO_2, respectively. The results presented above indicate the successfully construction of sea-urchin-like ReS_2 nanosheet/TiO_2 nanoparticle heterojunctions. With the presence of the above heterojunction interface, the light-induced charges can transfer from TiO_2 to sea-urchin-like ReS_2 nanosheets, then rapidly move to 2D planar edges/tips of urchin-like ReS_2 nanosheets due to the charge edge-collection effect, thus accelerating the separation and transfer

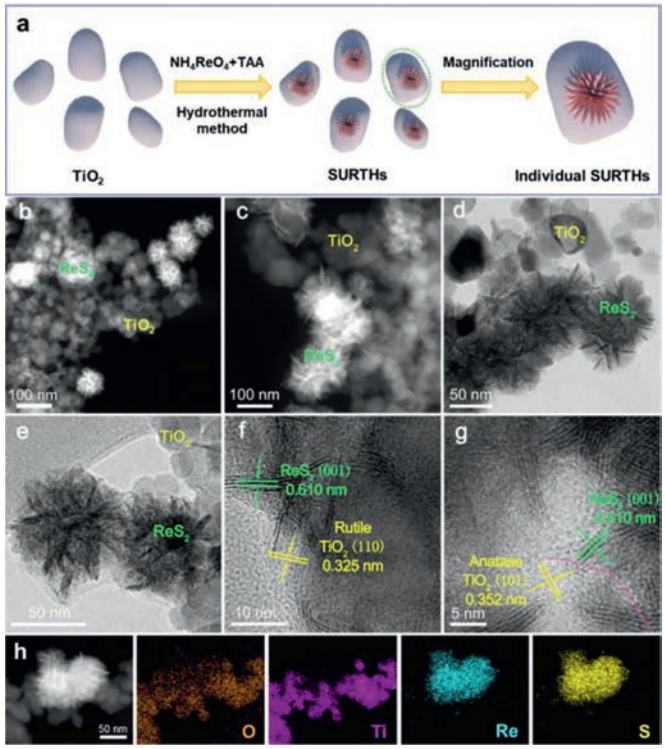

Fig. 1. (a) The formation procedure of SURTHs. (b, c) HAADF-STEM, (d, e) TEM and (f, g) HRTEM images of SURTHs. (h) HAADF-STEM and corresponding mapping images of O, Ti, Re and S.

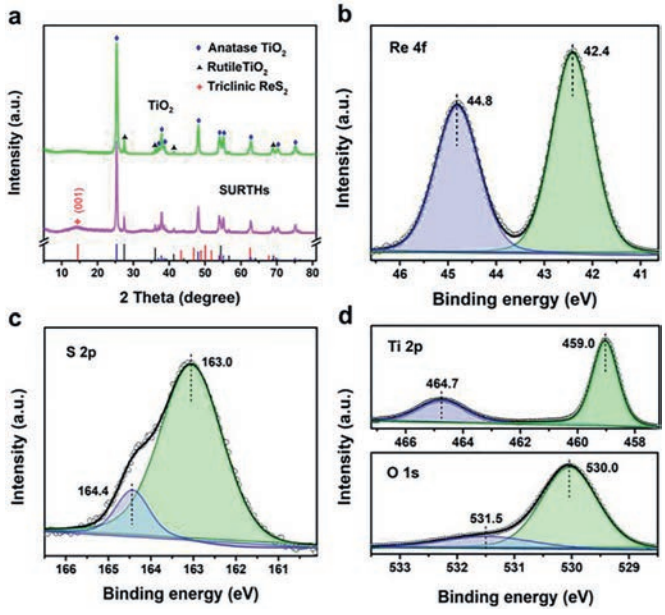

Fig. 2. (a) XRD patterns of TiO_2 and SURTHs. XPS spectra of SURTHs in the regions of (b) Re 4f, (c) S 2p, (d) Ti 2p and O 1s.

of charges significantly. This conclusion is strongly supported by the elemental mappings (Fig. 1h) and the energy-dispersive X-ray (EDX) images (Fig. S1 in Supporting information), where SURTHs exhibits the uniform spatial distribution of the elements of O, Ti, Re, and S.

Fig. 2a shows the X-ray diffraction (XRD) patterns of P25 TiO_2 (shorthand for TiO_2) and SURTHs. Concerning TiO_2, all XRD diffraction peaks are assigned to the anatase and rutile crystal structures of TiO_2 (JCPDS No. 21-1272 and No. 21–1276) [23]. For the XRD

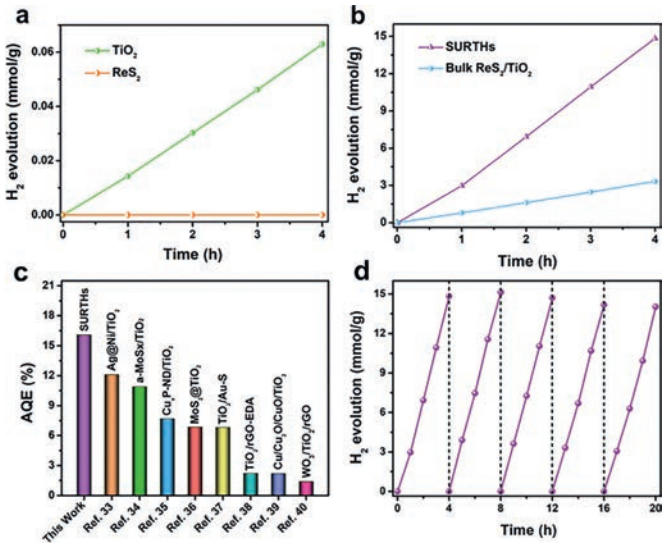

Fig. 3. (a) Time-dependent photocatalytic hydrogen production of TiO_2 and ReS_2 under simulated solar-light irradiation. (b) Time-dependent photocatalytic hydrogen production of Bulk ReS_2/TiO_2 and SURTHs under simulated solar-light irradiation. (c) Wavelength-dependent AQE at 365 nm for photocatalytic hydrogen production over SURTHs in this work by contrast with the previously reported work of TiO_2-based photocatalysts. (d) Cycling tests for hydrogen production over SURTHs under simulated solar-light irradiation.

curve of SURTHs, a minor and broad peak at 14.4° corresponds to the (001) crystal plane of triclinic ReS_2 (JCPDS No. 27-0502) [24,25], and all other XRD peaks are attributed to the anatase and rutile crystal structures of TiO_2, strongly suggesting the formation of ReS_2/TiO_2 heterojunctions. To further study the surface chemical state of SURTHs, the X-ray photoelectron spectroscopy (XPS) was performed. As shown in Fig. 2b, the peaks in the Re 4f region at 42.4 and 44.8 eV belong to Re $4f_{7/2}$ and Re $4f_{5/2}$ in ReS_2, respectively [13,14,26]. The peaks in the S 2p region (Fig. 2c) at 163.0 and 164.4 eV are attributed to S $2p_{3/2}$ and S $2p_{1/2}$ in ReS_2, respectively [14,27,28]. The peaks in the Ti 2p region (Fig. 2d) at 459.0 and 464.7 eV are ascribed to Ti $2p_{3/2}$ and Ti $2p_{1/2}$ in TiO_2, respectively [29,30]. The peaks in the O 1s region (Fig. 2d) indicate the presence of Ti–O bond at 530.0 eV and O–H bond at 531.5 eV [31,32]. The XPS results presented above strongly indicate the formation of urchin-like ReS_2 nanosheets with the charge edge-collection effect on the surface of TiO_2 nanoparticles.

Time-dependent photocatalytic hydrogen production experiments were performed using triethanolamine as the hole scavenger under simulated solar-light irradiation. As exhibited in Fig. 3a, pure ReS_2 exhibits the negligible photocatalytic hydrogen evolution rate (HER), while TiO_2 shows a far low HER of 0.016 mmol h^{-1} g^{-1}, indicative of their inferior charge-separation capacity. With the construction of the ReS_2/TiO_2 heterojunctions, the sample of bulk ReS_2/TiO_2 nanoparticle heterojunctions (bulk ReS_2/TiO_2, Fig. 3b and Fig. S2 in Supporting information) shows sharply increased HER of 0.83 mmol h^{-1} g^{-1}, indicative of the advantages of the heterojunction interface. As expected, SURTHs with the optimal cocatalyst-loading amount displays a remarkable performance with a HER of 3.71 mmol h^{-1} g^{-1} (Fig. 3b and Fig. S3 in Supporting information), up to 4.47 and 231.9 times by contrast with that of bulk ReS_2/TiO_2 and TiO_2, respectively, suggesting the high photocatalytic activity induced by the sea-urchin-like structured ReS_2 cocatalyst with charge edge-collection effect. The AQE of SURTHs was estimated to be 16.09% at 365 ± 10 nm (Fig. 3c), far outperforming the overwhelming majority of TiO_2-based photocatalysts as previously reported [33-40]. The stability of hydrogen production for SURTHs was investigated. As shown in Fig. 3d, SURTHs displays a negligible photoactivity loss after 5 consecutive cycling tests, suggesting its excellent stability, as evidenced by the XRD patterns in Fig. S4 (Supporting information), where the XRD patterns of fresh SURTHs and recycled SURTHs show no obvious differences. Additionally, HAADF-STEM, TEM and HRTEM images of the SURTHs sample after the 5th reaction (Fig. S5 in Supporting information) further support the above results, where the recycled SURTHs remains the relatively intact structure of sea-urchin-like ReS_2 nanosheet/TiO_2 nanoparticle heterojunctions similarly to the fresh SURTHs in Figs. 1b-g.

To reveal the dominating factors regarding the outstanding photocatalytic H_2 evolution performance of sea-urchin-like ReS_2 nanosheet/TiO_2 nanoparticle heterojunctions, the optical properties, textural properties and photoelectronic properties of SURTHs were investigated. In the UV–vis diffuse reflectance spectra (DRS, Fig. S6a in Supporting information), TiO_2 displays an absorption in the ultraviolet region with a calculated band-gap energy (E_g) of 3.19 eV. Notably, SURTHs shows a dramatically enhanced visible-light absorption than TiO_2 due to the effect of ReS_2. The ultraviolet photoelectron spectroscopy (UPS) was carried out to investigate the details of energy-band structure of TiO_2. As exhibited in Fig. S6b (Supporting information), according to the UPS excitation energy of 21.22 eV, the valence band energy (E_v) of TiO_2 concerning the vacuum level is calculated to be −7.27 eV, and the conduction band energy (E_c) of TiO_2 is calculated to be −4.08 eV based on its E_g value. It is noted that 0 V *versus* the normal hydrogen electrode (NHE) equals to −4.44 eV *versus* the vacuum level, therefore, the E_v and E_c of TiO_2 regarding the NHE are estimated to be 2.83 V and −0.36 V, respectively. Moreover, the N_2 adsorption-desorption isotherms of TiO_2 and SURTHs were measured to acquire the texture information. As showed in Fig. S6c (Supporting information), both of TiO_2 and SURTHs display the typical IV adsorption-desorption isotherm of N_2 with a H3-type hysteresis loop, suggesting the existence of mesopores [41–43]. This result is well supported by the pore-size distributions in Fig. S6d (Supporting information), where both of TiO_2 and SURTHs exhibit a pore-size distribution in the region of 2–100 nm, suggesting the coexistence of mesopores and macropores. The specific surface areas and pore volumes of TiO_2 and SURTHs are displayed in Table S1 (Supporting information). It can be found that SURTHs exhibits slightly increased specific surface area (35.78 m^2/g) and pore volume (0.25 cm^3/g) by contrast with those of TiO_2 (30.09 m^2/g and 0.14 cm^3/g, respectively), which can be attributed to the introduction of sea-urchin-like ReS_2 nanosheets.

To investigate the separation and migration capacity of charges, transient photocurrent responses of TiO_2 and SURTHs were detected. As shown in Fig. 4a, SURTHs displays a high photocurrent density of 1.45 $\mu A/cm^2$, up to 2.07 times higher than TiO_2 (0.70 $\mu A/cm^2$), indicative of significantly accelerated separation and transfer of charges [44–48]. This result is proved by the electrochemical impedance spectroscopy (EIS). As displayed in Fig. 4b, SURTHs exhibits a far smaller radius of Nyquist circle by contrast with TiO_2, suggestive of the advantages of the unique ReS_2 cocatalyst with the sea-urchin-like structure on accelerating charge transfer [49–51]. Photoluminescence (PL) spectra (Fig. 4c) further support the results presented above, where SURTHs displays a lower emission peak intensity by contrast with TiO_2, indicating the promotion of charge separation [52–55]. Additionally, the time-resolved fluorescence decay spectrum is powerful technique for probing the charge-transfer dynamics. It can be found in Fig. 4d that both of fluorescence spectra for TiO_2 and SURTHs display an exponential intensity decay. The relative fluorescence lifetimes of charge carriers were obtained by fitting the kinetics with two-exponential decay functions. As displayed in Table S2 (Supporting information), the average fluorescence lifetime of charge carriers significantly increases from TiO_2 (3.64 ns) to SURTHs (6.67 ns),

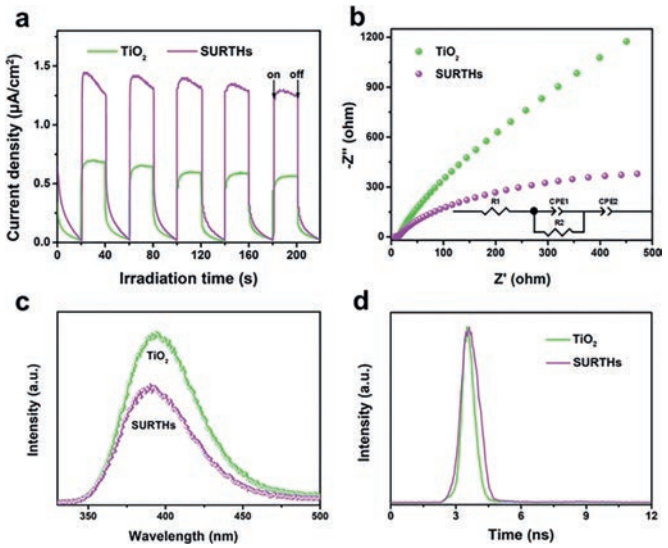

Fig. 4. (a) Transient photocurrent responses of TiO_2 and SURTHs. (b) EIS Nyquist plots of TiO_2 and SURTHs. The inset in (b) displays the impedance equivalent circuit. (c) PL spectra of TiO_2 and SURTHs. (d) Time-resolved fluorescence decay spectra of TiO_2 and SURTHs.

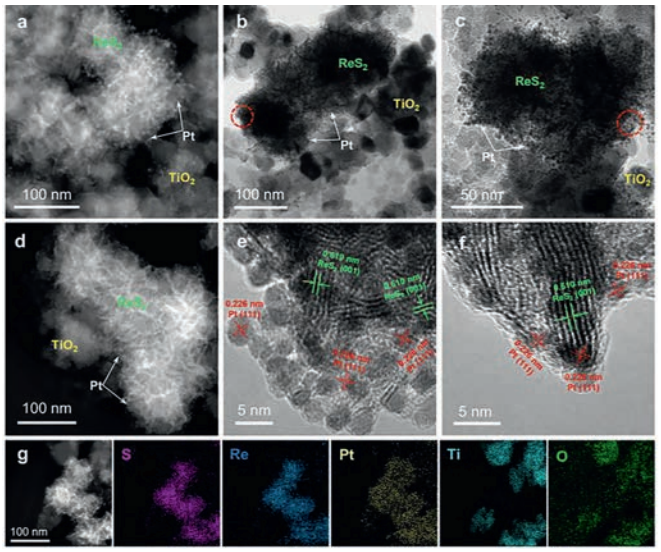

Fig. 5. (a, d) HAADF-STEM images of Pt quantum dots/SURTHs. (b, c) TEM images of Pt quantum dots/SURTHs. (e, f) HRTEM images of Pt quantum dots/SURTHs. The images of (e) and (f) correspond to the areas of the red dotted circles in (b) and (c), respectively. (g) HAADF-STEM and corresponding mapping images of S, Re, Pt, Ti and O.

strongly suggesting that the sea-urchin-like ReS_2 nanosheets with the charge edge-collection effect can facilitate the charge transfer and prolong the radiative lifetime of charge carriers for SURTHs [56–60]. Based on all the results presented in Fig. S6 (Supporting information) and Fig. 4, we can draw a conclusion that the excellent performance for photocatalytic H_2 evolution of SURTHs is mainly attributed to the significantly improved charge separation and transfer capacity induced by the unusual cocatalyst of sea-urchin-like ReS_2 nanosheets with the charge edge-collection effect.

In order to shed light on the charge edge-collection effect of sea-urchin-like ReS_2 nanosheets in SURTHs, we elaborated the photodeposited experiments of Pt quantum dots on the surface of SURTHs with H_2PtCl_6 and triethanolamine as the precursor and the hole scavenger, respectively. It is noteworthy that the photoexcited electrons arriving from TiO_2 in SURTHs can reduce the $[PtCl_6]^{2-}$ to Pt quantum dots under simulated solar-light irradiation, hence, we can almost determine the collection location of photoexcited electrons in SURTHs through investigating the spatial distribution of photodeposited Pt quantum dots. As shown in Figs. 5a and d, the HAADF-STEM images reveal that lots of Pt quantum dots like bright spots are mainly decorated on the edges/tips of sea-urchin-like ReS_2 nanosheets in SURTHs. The TEM images in Figs. 5b and c well evidence the results of the HAADF-STEM images, where Pt quantum dots are preferentially loaded on the edges/tips of sea-urchin-like ReS_2 nanosheets rather than randomly distributed on the whole surface of SURTHs. Furthermore, the HRTEM images in Figs. 5e and f further indicate that numerous Pt quantum dots with a size of ~4 nm were collected at the sharp edges/tips of sea-urchin-like ReS_2 nanosheets, strongly confirming the charge edge-collection effect of sea-urchin-like ReS_2 nanosheets in SURTHs. Additionally, the mapping images (Fig. 5g) and the EDX image (Fig. S7 in Supporting information) support the results mentioned above, where the element of Pt exhibits the similar spatial distribution with the elements of S and Re in the sample of Pt quantum dots/SURTHs, again evidencing the charge edge-collection effect.

According to all the results mentioned above, an underlying mechanism for the improvement of photocatalytic H_2 evolution activity has been proposed. Under the simulated solar-light irradiation ($\lambda \geq 300$ nm), TiO_2 in SURTHs can be excited to generate photoexcited electrons and holes (Figs. S6a and b) [61]. The photoexcited holes are consumed by the hole-scavenger, while the photoexcited electrons transfer to the ReS_2 cocatalyst and reduce the H^+ in aqueous solution to generate H_2 [62,63]. Notably, the sea-urchin-like ReS_2 nanosheet with the charge edge-collection effect is responsible for the excellent photocatalytic activity of SURTHs. As illustrated in the above well-designed experiment of selectively photodeposited Pt quantum dots in SURTHs (Fig. 5), the overall sea-urchin-like ReS_2 nanosheets are consisted of numerous open-up interconnecting minor sheets with sharp edges like the spines of a sea urchin (Scheme 1), which can enable the photoexcited electrons arrived at the ReS_2 cocatalyst to transfer towards the sharp edges/tips rapidly, similarly to the working principle of the lightning rods, thus achieving a significantly acceleration of charge transfer (Fig. 4) and a high HER performance of 3.71 mmol h^{-1} g^{-1} (an AQE of 16.09%) for SURTHs.

In summary, novel sea-urchin-like ReS_2 nanosheet/TiO_2 nanoparticle heterojunctions were successfully synthesized using a simple one-step hydrothermal method. Through the well-designed experiment regarding the selective photodeposition of Pt quantum dots, we unravel the unique charge edge-collection effect in the cocatalyst of sea-urchin-like ReS_2 nanosheets. Due to the charge edge-collection effect of sea-urchin-like ReS_2 nanosheets, the charge separation and transfer of SURTHs is accelerated significantly, thus yielding a high photocatalytic H_2 evolution rate of 3.71 mmol h^{-1} g^{-1} (an AQE of 16.09%), up to 231.9 times by contrast with that of P25 TiO_2.

Declaration of competing interest

The authors declare no conflict of competing interest.

Acknowledgments

This work was funded by the China Postdoctoral Science Foundation (pre-station, No. 2019TQ0050), Applied Basic Research Program of Sichuan Province (No. 2020YJ0068), the China Postdoctoral Science Foundation (No. 2020M673186), National Natural Science Foundation of China (No. 22002014), the Applied Basic Research Program of Sichuan Province (No. 2020ZYD014). Thanks for the technical help from Sichuan Province Key Laboratory of Display

Science and Technology, State Key Laboratory of Electronic Thin Films and Integrated Devices. Dr. Xiao Luo acknowledges financial support from the National Natural Science Foundation of China (No. 21903084) and Applied Basic Research Program of Sichuan Province (No. 2021YJ0408). Dr. Qing Liu acknowledges financial support from the National Natural Science Foundation of China (No. 52002051) and the Fundamental Research Funds for the Central Universities, SCUT (No. ZYGX2020J009).

Supplementary materials

Supplementary material associated with this article can be found, in the online version, at doi:10.1016/j.cclet.2021.07.015.

References

[1] V.W.H. Lau, V.W.Z. Yu, F. Ehrat, et al., Adv. Energy Mater. 7 (2017) 1602251.
[2] V.W. Lau, I. Moudrakovski, T. Botari, et al., Nat. Commun. 7 (2016) 12165.
[3] B. Lin, Z. Chen, P. Song, et al., Small 16 (2020) 2003302.
[4] C. Xue, P. Zhang, G. Shao, G. Yang, Chem. Eng. J. 398 (2020) 125602.
[5] W. Bi, X. Li, L. Zhang, et al., Nat. Commun. 6 (2015) 8647.
[6] B. Lin, H. An, X. Yan, et al., Appl. Catal. B: Environ. 210 (2017) 173–183.
[7] S. Bai, L. Yang, C. Wang, et al., Angew. Chem. Int. Ed. 54 (2015) 14810–14814.
[8] L. Li, Z. Deng, L. Yu, et al., Nano Energy 27 (2016) 103–113.
[9] H. Zhang, P. Zhang, M. Qiu, et al., Adv. Mater. 31 (2019) 1804883.
[10] J. Yu, S. Seo, Y. Luo, et al., ACS Nano 14 (2020) 1715–1726.
[11] Q. Lu, Y. Yu, Q. Ma, B. Chen, H. Zhang, Adv. Mater. 28 (2016) 1917–1933.
[12] J. Zhou, J. Lin, X. Huang, et al., Nature 556 (2018) 355–359.
[13] J. Ran, H. Zhang, J. Qu, et al., ACS Mater. Lett. 2 (2020) 1484–1494.
[14] X. Wang, B. Chen, D. Yan, et al., ACS Appl. Mater. Interfaces 11 (2019) 23144–23151.
[15] J. Zhang, M. Zhang, C. Yang, X. Wang, Adv. Mater. 26 (2014) 4121–4126.
[16] C. Sun, H. Zhang, H. Liu, et al., Appl. Catal. B: Environ. 235 (2018) 66–74.
[17] W. Wang, S. Zhu, Y. Cao, et al., Adv. Funct. Mater. 29 (2019) 1901958.
[18] J. Ran, J. Zhang, J. Yu, M. Jaroniec, S.Z. Qiao, Chem. Soc. Rev. 43 (2014) 7787–7812.
[19] L. Kong, Y. Ji, Z. Dang, et al., Adv. Funct. Mater. 28 (2018) 1800668.
[20] Y.X. Pan, J.B. Peng, S. Xin, et al., ACS Sustain. Chem. Eng. 5 (2017) 5449–5456.
[21] H. Liu, Q. Zhao, H. Zhou, et al., Phys. Chem. Chem. Phys. 13 (2011) 10872–10876.
[22] Y. Yang, G. Zhuang, L. Sun, et al., J. Mater. Chem. A 8 (2020) 17449–17453.
[23] T. Wang, X. Yan, S. Zhao, et al., J. Mater. Chem. A 2 (2014) 15611–15619.
[24] N.A. Dulaimi, D.J. Lewis, X.L. Zhong, M.A. Malik, P. O'Brien, J. Mater. Chem. C 4 (2016) 2312–2318.
[25] A. Yella, H.A. Therese, N. Zink, M. Panthofer, W. Tremel, Chem. Mater. 20 (2008) 3587–3593.
[26] J. Borowiec, W. Liang, F.S. Boi, et al., Chem. Eng. J. 392 (2020) 123745.
[27] Y. Zhou, E. Song, J. Zhou, et al., ACS Nano 12 (2018) 4486–4493.
[28] B. Lin, A. Chaturvedi, J. Di, et al., Nano Energy 76 (2020) 104972.
[29] X. Yu, J. Huang, J. Zhao, et al., Chem. Eng. J. 403 (2021) 126359.
[30] X. Liu, Y. Zhang, S. Matsushima, H. Hojo, H. Einaga, Chem. Eng. J. 402 (2020) 126220.
[31] Z. Jiao, M. Shang, J. Liu, et al., Nano Energy 31 (2017) 96–104.
[32] Y. Zhang, J. Liu, Y. Zhang, Y. Bi, Nano Energy 51 (2018) 504–512.
[33] D. Gao, W. Liu, Y. Xu, et al., Appl. Catal. B: Environ. 260 (2020) 118190.
[34] H. Yu, R. Yuan, D. Gao, Y. Xu, J. Yu, Chem. Eng. J. 375 (2019) 121934.
[35] J. Xu, W. Zhong, H. Yu, et al., J. Mater. Chem. C 8 (2020) 15816–15822.
[36] X. Hu, S. Lu, J. Tian, et al., Appl. Catal. B: Environ. 241 (2019) 329–337.
[37] P. Wang, Y. Cao, S. Xu, H. Yu, Appl. Surf. Sci. 532 (2020) 147420.
[38] H. Li, P. Wang, X. Yi, H. Yu, Appl. Catal. B: Environ. 264 (2020) 118504.
[39] Z. Zhang, K. Liu, Y. Bao, B. Dong, Appl. Catal. B: Environ. 203 (2017) 599–606.
[40] F. He, A. Meng, B. Cheng, W. Ho, J. Yu, Chin. J. Catal. 41 (2020) 9–20.
[41] B. Lin, H. Li, H. An, et al., Appl. Catal. B: Environ. 220 (2018) 542–552.
[42] T. Cui, J. Dong, X. Pan, et al., J. Energy Chem. 28 (2019) 123–127.
[43] K. Qi, R. Selvaraj, T.A. Fahdi, et al., Appl. Surf. Sci. 387 (2016) 750–758.
[44] C. Xue, H. An, G. Shao, G. Yang, Chin. J. Catal. 42 (2021) 583–594.
[45] J. Di, J. Xiong, H. Li, Z. Liu, Adv. Mater. 30 (2018) 1704548.
[46] J. Liu, P. Wang, W. Qu, et al., Appl. Catal. B: Environ. 257 (2019) 117880.
[47] W. Ou, J. Pan, Y. Liu, et al., J. Energy Chem. 43 (2020) 188–194.
[48] B. Lin, Y. Zhou, B. Xu, et al., Mater. Horiz. 8 (2021) 612–618.
[49] Y. Zhou, J. Zhang, E. Song, et al., Nat. Commun. 11 (2020) 2253.
[50] D. Zhu, Q. Zhou, Appl. Catal. B: Environ. 281 (2021) 119474.
[51] J. Li, B. Huang, Q. Guo, et al., Appl. Catal. B: Environ. 284 (2021) 119733.
[52] K. Qi, S. Liu, M. Qiu, Chin. J. Catal. 39 (2018) 867–875.
[53] K. Qi, W. Lv, I. Khan, S. Liu, Chin. J. Catal. 41 (2020) 114–121.
[54] Y. Xing, X. Wang, S. Hao, et al., Chin. Chem. Lett. 32 (2021) 13–20.
[55] S. Sun, H. Ding, L. Mei, et al., Chin. Chem. Lett. 31 (2020) 2287–2294.
[56] J. Di, J. Xia, M.F. Chisholm, et al., Adv. Mater. 31 (2019) 1807576.
[57] B. Lin, G. Yang, L. Wang, Angew. Chem. Int. Ed. 58 (2019) 4587–4591.
[58] J. Di, P. Song, C. Zhu, et al., ACS Mater. Lett. 2 (2020) 1025–1032.
[59] B. Lin, H. Chen, Y. Zhou, et al. , Chin. Chem. Lett. 32 (2021) 3128–3132.
[60] K. Qi, F. Zasada, W. Piskorz, et al., J. Phys. Chem. C 120 (2016) 5442–5456.
[61] R. Wang, C. He, W. Chen, C. Zhao, J. Huo, Chin. Chem. Lett. (2021), doi:10.1016/j.cclet.2021.05.024.
[62] H. Yang, C. He, L. Fu, et al. , Chin. Chem. Lett. 32M (2021) 3202–3206.
[63] L. Fu, R. Wang, C. Zhao, et al., Chem. Eng. J. 414 (2021) 128857.